Systems & Control Transactions

Research Article - Peer Reviewed Conference Proceeding
ESCAPE 35 - European Symposium on Computer Aided Process Engineering
Ghent, Belgium. 6-9 July 2025
Jan F.M. Van Impe, Grégoire Léonard, Satyajeet S. Bhonsale,
Monika E. Polańska, Filip Logist (Eds.)

PSE PRESS

Numerical Modelling of Carbon Dioxide Adsorption in Dual Function Materials: An CFD approach.

Andrés F. Soto-Cañón[a], Rodinson R. Arrieta-Peréz[a], Camilo Rengifo[b], Martha Cobo[a] and Manuel Figueredo[a,*]

[a] Universidad de La Sabana, Department of Chemical Engineering, Chía, Cundinamarca, Colombia
[b] Universidad de La Sabana, Department of Mathematics, Physics and Statistics, Chía, Cundinamarca, Colombia
* Corresponding Author: manuel.figueredo@unisabana.edu.co

ABSTRACT

Integrated Carbon Capture and Conversion (ICCC) technologies offer an efficient alternative to conventional Carbon Capture, Utilization, and Storage (CCUS) methods by simultaneously capturing and converting CO_2 into value-added chemicals. Dual-function materials (DFMs) are particularly promising due to their capability to integrate adsorption and catalysis in a single step, thereby reducing both energy consumption and associated costs. This study models the dynamic behavior of CO_2 adsorption within a laboratory-scale packed-bed reactor employing DFMs. The mathematical model incorporates momentum, mass, and heat transfer equations, implemented using COMSOL Multiphysics v5.6, and evaluates various axial dispersion models (ADMs) and mass transfer coefficients (MTCs). The results indicate that the Rastegar-Gu ADM, combined with an MTC of 8.3×10^{-2} s^{-1}, provides the most accurate representation of breakthrough and saturation times, as well as the total quantity adsorbed. Furthermore, relative errors associated with this model are consistently lower than those observed in alternative models. These findings offer valuable insights for the scaling-up of ICCC technologies, underscoring the significance of precise Computational Fluid Dynamics (CFD) simulations in advancing sustainable CO_2 capture and conversion solutions.

Keywords: Adsorption, Carbon Capture, Computational Fluid Dynamics, DFMs

INTRODUCTION

ICCC technologies represents an advancement over conventional CCUS methods[1]. The ICCC technologies are based on the *in-situ* conversion of the captured carbon into high-value chemical products, such as methane and methanol, thus eliminating the need for costly compression and transport processes [1]. Among these technologies, DFMs emerge as a promising solution, facilitating the integration of CO_2 adsorption (capture) and methanation (conversion), while simultaneously reducing energy consumption [2].

However, there remains a gap between the research and development of DFMs and their industrial implementation [1, 2]. As a result, both numerical simulation and CFD are pivotal in the optimal design and scale-up of these processes.

In the context of carbon dioxide adsorption, the numerical simulation incorporates the three primary transport phenomena – momentum, mass and heat transfer- coupled with equilibrium and kinetic adsorption models [3]. This approach is suitable for a range of adsorbent materials and their modifications [4]. Additionally, numerical simulation offers a rigorous framework for the design and optimal mathematical description for cyclic carbon capture processes, such as Pressure Swing Adsorption (PSA) and Temperature Swing Adsorption (TSA) [5].

The dynamic behavior of the adsorption column is typically described by a “breakthrough curve”. This curve is generated as the mass transfer zone advances through the column and reaches the exit [6]. The shape of the mass transfer zone and, consequently the breakthrough curve, depends on the isotherm model, axial dispersion model, and mass transfer model [7].

Both the axial dispersion coefficient and the mass transfer coefficient are key parameters influencing the adsorption dynamic behavior [8]. Axial dispersion arises from turbulent mixing and molecular diffusion [4, 6]

The mass transfer coefficient reflects the rate at which the adsorbate is transferred from the gas phase to the solid phase within the particles. It may also account for the resistance effects associated with diffusion into the solid materials [6].

In this study, the dynamic behavior of carbon dioxide adsorption from a nitrogen mixture using a $Ru/Na_2O_3/Al_2O_3$ DFM in a laboratory-scale packed bed is simulated using COMSOL Multiphysics v5.6. The momentum, mass, and heat transfer phenomena are modeled and integrated through various physics modules. Furthermore, several axial dispersion models (ADM) and mass transfer coefficients (MTCs) are evaluated.

MATHEMATICAL MODELS

This section presents the formulation of the mathematical model. It outlines the assumptions, the geometry implemented in the software, and the physics modules, along with the equations utilized.

Assumptions

For simplicity, several assumptions have been made regarding the mathematical model. First, it is assumed that only carbon dioxide is adsorbed onto the DFM, and the linear driving force model is implemented to account for mass loss. Additionally, the gas mixture is considered ideal. Finally, the energy balance model is assumed to be homogeneous.

Geometry

To replicate the experimental system, a one-dimensional geometry was created in COMSOL along de *x*-axis. Two subdomains were defined: quartz wool and DFM. Figure 1 illustrates the final geometry implemented in the CFD model, while Image 1 depicts the laboratory-scale reactor used in the experiment.

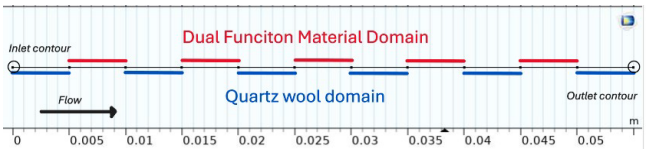

Figure 1. One-dimensional geometry employed in COMSOL.

Image 1. Laboratory-scale DFM packed reactor employed.

Governing transport phenomena equations

Momentum Balance

For the momentum balance, Darcy's *Law* physics module was implemented. This module includes both the continuity equation and the Darcy's law equation for pressure drop. The equation is expressed as follows:

$$\frac{\partial(e_{cat}\rho_f)}{\partial t} + \frac{\partial}{\partial x}\rho_f u = 0 \quad (1)$$

$$u = -\frac{\varkappa}{\mu}\frac{\partial P}{\partial x} \quad (2)$$

Where: u is the Darcy velocity (m/s), e_{cat} is the DFM porosity, ρ_f and μ represent the gas phase density (kg/m^3) and viscosity (Pa·s), respectively. Finally, $\varkappa$ is the permeability (m^2), which was calculated using the integrated Kozeny-Carman equations and P is pressure (Pa).

Mass Balance

The Mass balance equations were modeled using *transport of diluted species* physics modules. The equation is expressed as follows.

$$\frac{\partial C_i}{\partial t} - D_L\frac{\partial^2 C_i}{\partial x^2} + u\frac{\partial C_i}{\partial x} = \mathrm{R}_i \quad (3)$$

Where C_i denotes the gas phase concentration of each species (mol/m^3), D_L represents the axial dispersion coefficient (m^2/s), and R_i refers to the reaction or sink term (mol/m^3·s).

Adsorption term

To simulate the adsorption phenomenon, the linear driving force equation was implemented as a *domain ordinary differential equation* module, applied exclusively to the DFM subdomain.

$$\frac{\partial q}{\partial t} = k(q_e - q) \quad (4)$$

In this equation, q represents the quantity of carbon dioxide adsorbed onto the solid material (mol/kg), q_e is the equilibrium quantity (mol/kg), and k is the mass transfer coefficient (1/s).

Thus, the mass balance for carbon dioxide is expressed as follows:

$$\frac{\partial C_{CO_2}}{\partial t} - D_L\frac{\partial^2 C_{CO_2}}{\partial x^2} + u\frac{\partial C_{CO_2}}{\partial x} = -\frac{1-e_{cat}}{e_{cat}}\rho_s\frac{\partial q}{\partial t} \quad (5)$$

For nitrogen, R_i is equal to zero.

Adsorption equilibrium

The Langmuir isotherm model was used to represent the equilibrium quantity (equation 6). To ensure an accurate depiction of these phenomena, the model was fitted to experimental data obtained with a Micromeritics ASAP 2020+ at pressures up to 760 mmHg and 320 °C for Na_2O/Al_2O_3, a precursor to DFM. Table 1 presents the obtained parameters values.

$$q_e = \frac{q_{sat}K_L P_{CO_2}}{1+K_L P_{CO_2}} \quad (6)$$

Table 1: Langmuir isotherm model parameters.

Stream	Description	Value
q_{sat}	Saturated quantity	0.193 mol/kg
K_L	Equilibrium constant	$73x10^{-5}$ Pa^{-1}

Energy Balance

The energy balance was modeled using the *heat transfer on porous media* physics module. The equation is expressed as follows:

$$A_c(\rho C_p)_{eff}\frac{\partial T}{\partial t} + A_c\rho_f C_{p,f} u\frac{\partial T}{\partial x} - A_c k_{eff}\frac{\partial T^2}{\partial x^2} = Q_{ads} \quad (7)$$

Where: T is the system temperature (K), A_c the cross-sectional area (m^2), k_{eff} represents the effective heat transfer coefficient (W/m·K), and Q_{ads} denotes the heat of adsorption (W/m^3).

Boundary conditions

The equations for the boundary conditions at the boundaries of the geometry (Figure 1) are expressed as follows:

$$\boldsymbol{n}\cdot(\rho_f u) = \rho_f U_0 \quad (8)$$

$$\boldsymbol{n}\cdot\left(-D_L\frac{\partial C_i}{\partial x} + uC_i\right) = \boldsymbol{n}\cdot(uC_{i,0}) \quad (9)$$

$$-\boldsymbol{n}\cdot\left(-A_c k_{eff}\frac{\partial T}{\partial x}\right) = A_c\rho_f\Delta H(\boldsymbol{n}\cdot u) \quad (10)$$

Equations (8-10) represent the Danckwerts form for the inlet conditions for the momentum, mass, and energy balance, respectively. Here, U_0 is the initial Darcy velocity, $C_{i,0}$ the initial concentration of each gas in the inlet mixture (calculated using ideal gas equation), and ΔH the sensible enthalpy (KJ/mol) [9]

$$\boldsymbol{n} * (\rho_f u) = p_0 \quad (11)$$

$$\boldsymbol{n} * \left(-D_L\frac{\partial C_i}{\partial x}\right) = 0 \quad (12)$$

$$-\boldsymbol{n} * \left(-A_c k_{eff}\frac{\partial T}{\partial x}\right) = 0 \quad (13)$$

On the other hand, equations (11-13) describe the outlet boundary conditions. Here, p_0 represents the barometric pressure at the outlet, defined as zero. This condition ensures that *Darcy's Law* physics module calculates the barometric pressure drop [9].

Initial values

The initial values for each of the main transport equations are presented as follows:

$$p_{t=0} = p_{op} \quad (14)$$

$$C_{CO_2,t=0} = 0 \qquad C_{N_2,t=0} = \frac{p_{op}}{R*T_{op}} \quad (15)$$

$$q_{CO_2,t=0} = 0 \quad (16)$$

$$T_{t=0} = T_{op} \quad (17)$$

Where: p_{op} is the initial barometric pressure and T_{op} is the initial temperature.

Mixture properties calculation

The mixture properties, including density, viscosity, heat capacity and thermal conductivity, were calculated using a thermodynamics module. Each property was modeled as a function of temperature, pressure, and molar composition. However, to reduce computational time, these calculations were based on the inlet mixture compositions and a constant inlet barometric pressure.

Computational aspects

As previously mentioned, COMSOL Multiphysics v5.6 CFD software was used. A mesh of ninety-nine (99) elements was created in conjunction with the one-dimensional geometry. A dynamic study was conducted from 0 to 540 seconds. MATLAB was employed as complemented software to perform various calculations.

METHODOLOGY

Axial dispersion coefficient models

Several models were evaluated to identify the most suitable for representing the dynamic behavior of the adsorption process. These models, along with their respective equations, are presented in the table below:

Table 2: Axial dispersion models evaluated.

Model	Equation
No model (NM)	$D_L = D_m$
Wakao-Funazkri (WF)[6]	$D_L = \frac{D_m}{e_{cat}}(20 + 0.5ScRe)$
General model (GM) [6]	$D_L = 0.7D_m + 0.5dp_{cat}u$
Rastegar-Gu (RG) [4]	$D_L = \frac{d_{p,cat}u}{Pe_z}$ $\frac{1}{Pe_z} = \frac{0.7D_m}{Lu} + \frac{d_{p,cat}}{L}\frac{e_{cat}}{0.18+0.008Re^{0.59}}$

Mass transfer coefficient constants

Table 3 represents a list of evaluated mass transfer coefficient (MTC) constants.

Table 3: Mass transfer constants evaluated.

Reference	Value
[10]	$2.2\cdot10^{-2}$ [1/s]
[11]	$6.7\cdot10^{-2}$ [1/s]
[11]	$8.3\cdot10^{-2}$ [1/s]

The evaluation of both axial dispersion models (ADM) and mass transfer coefficient constants (MTC) were performed simultaneously by pairing each model

with its MTC. As a result, twelve tests were conducted, divided into three sets of simulations.

Table 4: Sets of simulations performed.

Set	Description
A	$k = 2.2 \cdot 10^{-2}$ [1/s]; with all ADM evaluated.
B	$k = 6.7 \cdot 10^{-2}$ [1/s]; with all ADM evaluated.
C	$k = 8.3 \cdot 10^{-2}$ [1/s]; with all ADM evaluated.

Breakthrough and saturation times

Two key design parameters for adsorption columns are the breakthrough t_b and saturation time t_s. These parameters correspond, respectively, to the time when the mass transfer zone reaches the end of the column and the time when the column is fully saturated or in equilibrium with the flowing gas [12].

These parameters will be compared to verify that the mathematical model can be extrapolated to the design and optimization of an industrial scale reactor.

Total quantity adsorbed

In addition to the t_b and t_s parameters, the total quantity adsorbed (q_{total}) is considered to assess the mathematical model and its relevance. Equation 18 presents the mathematical formula for its calculation [12].

$$q_{total} = \frac{F_{op} C_{i,in}}{m_{cat}} \int_0^{t_s} 1 - \frac{C_{i,out}(t)}{C_{i,in}} \partial t \quad (18)$$

Where: F_{op} is the volumetric flow (m³/s), $\frac{C_{i,out}(t)}{C_{i,in}}$ represents the breakthrough curve, and m_{cat} is the total mass of DFM inside the reactor (kg). To facilitate the rapid calculation of q_{total}, the breakthrough curve data for each run were first fitted to the Thomas model, as shown in Equation 19.

$$\frac{C(t)}{C_i} = \frac{1}{\exp\left(\frac{k_T q_T m_b}{F_{op}} - k_T C_i t\right) + 1} \quad (19)$$

By using the non-linear fitting tools in MATLAB, the values of k_T and q_T were determined. Subsequently, numerical integration was performed.

RESULTS

Breakthrough and saturation time

The breakthrough and saturation times obtained from the experimental set are presented in Table 5, while the results for each simulation set are shown in Tables 6-8.

To assess the accuracy of the simulation results, the relative error (RE) was calculated by comparing the simulated data with the corresponding experimental measurements. This comparison offers a quantitative evaluation of the model's predictive capability and underscores its potential reliability under the tested conditions.

Table 5: Experimental breakthrough and saturation times.

Set	t_b (min)	t_s (min)
Experimental	3.27	4.32

A comparison between the simulation results without the implementation of the ADM and the general model shows that the breakthrough and saturation times are closely aligned, both displaying similar trends of decreasing relative error as other mass transfer coefficient constants (MTC) are evaluated.

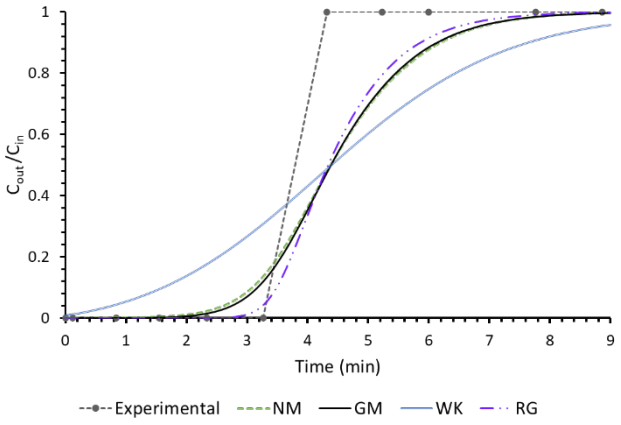

Figure 2. Axial dispersion model comparison. Set A

Table 6: Breakthrough and saturation times. Set A.

ADM	t_b (min)	RE t_b (%)	t_s(min)	RE t_s (%)
No Model	1.08	66.9	8.16	89.0
General Model	1.32	59.6	8.15	88.8
WK	0.017	99.5	11.1	157.1
RG	2.53	22.6	7.72	78.8

In contrast, the Rastegar-Gu model demonstrates a significant improvement over the previously discussed models. The application of this model results in more closely spaced breakthrough and saturation times, leading to a steeper breakthrough curve. This corresponds to a shorter mass transfer zone, a characteristic that must be accurately represented in a DFM-packed bed, as observed in the experimental breakthrough curves (Figure 2-4). Furthermore, the Rastegar-Gu model consistently exhibits the lowest relative error for both breakthrough and saturation times across all three simulation sets, offering superior predictive capability under the evaluated conditions.

The application of the Wakao-Funazkri model

results in a broader breakthrough curve, characterized by breakthrough times of less than 0.20 minutes and saturation times exceeding 9 minutes. Moreover, this model shows significantly high relative errors, approaching 100% when compared to experimental data. These results suggest that the model lacks the precision required to accurately represent the dynamics observed in the experimental setup.

From a different perspective, the use of mass transfer coefficient constants of $6.7 \cdot 10^{-2}$ s^{-1} and $8.3 \cdot 10^{-2}$ s^{-1} leads to a significant reduction in the relative error associated with both breakthrough and saturation times. For example, for the general model, the relative error in saturation time is reduced by half, as observed in the simulation without an implemented model. Moreover, the relative error for breakthrough times decreases substantially by nearly one-third for the case without any model implemented and by one-sixth for the general model.

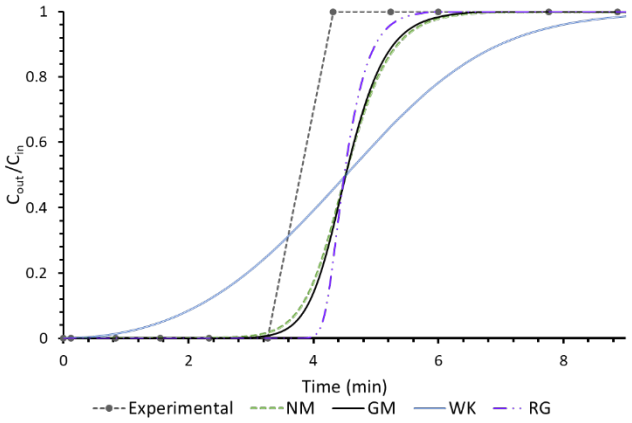

Figure 3. Axial dispersion model comparison. Set B

Table 7: Breakthrough and saturation times. Set B.

ADM	t_b (min)	RE t_b (%)	t_s(min)	RE t_s (%)
No Model	2.48	24.1	6.30	45.9
General	2.75	15.8	6.13	42.0
WK	0.12	96.3	9.33	116.1
RG	3.88	18.8	5.58	29.3

The most favorable results are obtained with a mass transfer coefficient constant of $8.3 \cdot 10^{-2}$ s^{-1}, combined with the Rastegar-Gu axial dispersion model. This combination demonstrates superior consistency, yielding comparable reductions in relative error for both breakthrough and saturation times.

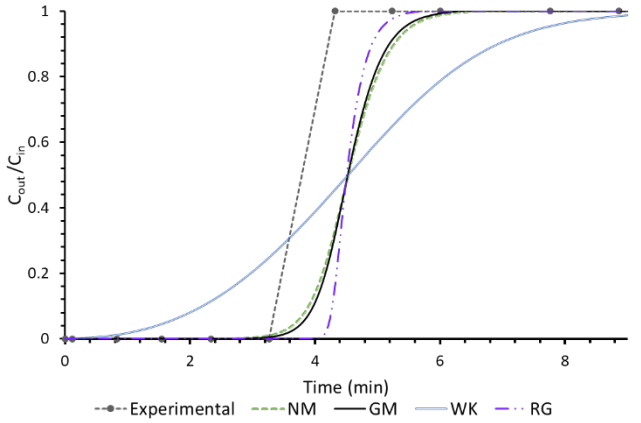

Figure 4. Axial dispersion model comparison. Set C

Table 8: Breakthrough and saturation times. Set C.

ADM	t_b (min)	RE t_b (%)	t_s(min)	RE t_s (%)
No Model	2.67	18.3	6.08	40.8
General	2.93	10.3	5.93	37.4
WK	0.18	94.5	9.20	113.1
RG	4.03	23.4	5.42	25.6

Total quantity adsorbed

Table 9: Experimental total quantity adsorbed.

Set	q_{total}(mmol/g)
Experimental	0.1645

The results for q_{total}, representing the total quantity adsorbed are presented in Table 9 for the experimental data and in Table 10 for each set of simulation runs. Due to the high relative errors observed, the Wakao-Funazkri axial dispersion model was excluded from the evaluation of q_{total}. This decision highlights the model's limitations in accurately representing the adsorption dynamics under the tested conditions, rendering it unsuitable for further analysis in this context.

Table 10: Results for the total quantity adsorbed for every set of runs.

Set	A	B	C
ADM		q_{total}(mmol/g)	
No model	0.1894	0.1926	0.1929
General	0.1893	0.1926	0.1929
Rastegar-Gu	0.1883	0.1920	0.1925

Table 11: Results for the relative error, comparison between experimental and simulated q_{total}.

Set	A	B	C
ADM		Relative error (%)	
No model	15.12	17.12	17.30
General	15.16	17.10	17.28
Rastegar-Gu	14.46	16.75	17.04

For all three simulation sets, the total quantity adsorbed exhibits only minor variations, with relative errors consistently around 15%. Regarding breakthrough and saturation times, the general model shows no significant improvement compared to simulations conducted without an implemented model. However, the Rastegar-Gu model remains the best option. In contrast to the behavior observed for breakthrough and saturation times, the relative error for q_{total} increases in simulation sets B and C. Despite this, the combination of the Rastegar-Gu axial dispersion model and a mass transfer coefficient constant of $8.3 \cdot 10^{-2}$ s^{-1} still provides the most accurate results in this context.

CONCLUSION

This study compares various axial dispersion models and mass transfer constants used in the mass balance model of a packed-bed adsorption column. Additionally, it provides valuable insights into the CFD simulation of the carbon dioxide adsorption process utilizing DFMs. The general model does not demonstrate significant improvement, as its results are comparable to those obtained from the simulation set where no axial dispersion coefficient model was applied.

The findings indicate that the Rastegar-Gu axial dispersion model, combined with MTC of $8.3 \cdot 10^{-2}$ s^{-1}, provides an effective approach for accurately replicating the adsorption behavior of DFMs. These results represent a crucial starting point for the design, optimization, and scaling of dual-function reactors, facilitating their further development in CO_2 capture and utilization technologies.

ACKNOWLEDGEMENTS

This project is funded by Ministry of Science, Technology, and Innovation (Minciencias, Patrimonio Autónomo del Fondo Nacional de Financiamiento Para la Ciencia, La Tecnología y la Innovación, Francisco José de Caldas) through the contract 441-2023.

REFERENCES

1. Bin S, et al. CO2 capture and in-situ conversion: recent progresses and perspectives. *GreenChE* 3:189-198 (2022) doi: 10.1016/j.gce.2021.11.009.
2. Han L, et al. Progress in reaction mechanisms and catalyst development of carbon dioxide methanation. *J CO2 Util* 84: 102845 (2024), doi: 10.1016/j.jcou.2024.102845.
3. Shuangjun L, et al. Mathematical modeling and numerical investigation of carbon capture by adsorption: Literature review and case study," *Appl Energy* 221: 437–449 (2018) doi: 10.1016/j.apenergy.2018.03.093.
4. Francisco J G O, Manuel B R, Ralph T Y. Modeling of fixed-bed columns for gas physical adsorption. *Chem. Eng. J* 378:121985 (2019) doi: 10.1016/j.cej.2019.121985.
5. Toluleke E A, Phebe L B P, Meihong W. Experimental studies, molecular simulation and process modelling\simulation of adsorption-based post-combustion carbon capture for power plants: A state-of-the-art review. *Appl Energy* 317:119156 (2022) doi: 10.1016/j.apenergy.2022.119156.
6. Douglas M. R, PRINCIPLES OF ADSORPTION AND AD-SORPTION PROCESSES. Wiley-Interscience, (1984).
7. Ralph T Y, GAS SEPARATION PROCESS BY ADSORPTION PROCESSES. Butterworth Publishers, (1987).
8. Motoyuki S. ADSORPTION ENGINEERING. Elsevier science (1990).
9. COMSOL Reference Manual https://www.comsol.com
10. Mingheng L. Dynamics of CO2 adsorption on sodium oxide promoted alumina in a packed-bed reactor. *Chem Eng Sci* 66:5938–5944 (2011) doi: 10.1016/j.ces.2011.08.013.
11. K. B. Lee, M. G. Beaver, H. S. Caram,S. Sircar. Chemisorption of carbon dioxide on sodium oxide promoted alumina. *AIChE Journal* 53:2824–2831, (2007) doi: 10.1002/aic.11312.
12. Alan G. Adsorption basics: part 1. *AIChE CEP* 48–53 (2017).